

Compositional modulation and surface stability in InGaP films: Understanding and controlling surface properties

J. R. R. Bortoleto, H. R. Gutiérrez, M. A. Cotta, and J. Bettini

Citation: *Journal of Applied Physics* **101**, 064907 (2007); doi: 10.1063/1.2712159

View online: <http://dx.doi.org/10.1063/1.2712159>

View Table of Contents: <http://scitation.aip.org/content/aip/journal/jap/101/6?ver=pdfcov>

Published by the [AIP Publishing](#)



Re-register for Table of Content Alerts

Create a profile.



Sign up today!



Compositional modulation and surface stability in InGaP films: Understanding and controlling surface properties

J. R. R. Bortoleto,^{a)} H. R. Gutiérrez,^{b)} and M. A. Cotta

Instituto de Física Gleb Wataghin, DFA, UNICAMP, CP 6165, 13083-970 Campinas-SP, Brazil

J. Bettini

Laboratório Nacional de Luz Síncrotron, CP 6192, 13084-971, Campinas-SP, Brazil

(Received 21 May 2006; accepted 19 January 2007; published online 23 March 2007)

We investigate the formation of compositional modulation and atomic ordering in InGaP films. Such bulk properties—as well as surface morphologies—present a strong dependence on growth parameters, mainly the V/III ratio. Our results indicate the importance of surface diffusion and, particularly, surface reconstruction for these processes. Most importantly from the application point of view, we show that the compositional modulation is not necessarily coupled to the surface instabilities, so that smooth InGaP films with periodic compositional variation could be obtained. This opens a new route for the generation of templates for quantum dot positioning and three-dimensional arrays of nanostructures. © 2007 American Institute of Physics.

[DOI: [10.1063/1.2712159](https://doi.org/10.1063/1.2712159)]

I. INTRODUCTION

One of the major interests in ternary and quaternary semiconductor alloys has been the ability to continuously vary the energy gap and strain through changes in composition in order to achieve advantageous band structure for opto- and microelectronic devices. For example, the ternary InGaP alloys have an enormous interest for applications in visible light emitters and tandem solar cells.¹ Furthermore, the engineering of strained layers has been successfully used as a method to control the lateral positioning of self-assembled quantum dots on the surface.^{2–4}

However, the successful performance of such devices depends on the ability to control both bulk and surface properties of these alloys on a particular substrate. A random atomic distribution in the semiconductor alloys could be assumed in a simple approach; however, in practice more complex phenomena as compositional variation and atomic ordering have been observed for different epitaxial techniques. For example, atomic ordering is present in InGaAs alloys grown by chemical vapor deposition (CVD),⁵ as well as InGaP films grown by both vapor phase epitaxy (VPE)^{6,7} and molecular beam epitaxy (MBE).⁸ Compositional modulation has been first observed for InGaAsP semiconductor alloys grown by liquid phase epitaxy (LPE).^{9,10} However, this bulk phenomenon is not limited to quaternary alloys or to the LPE growth technique. Several works have reported compositional modulation on other semiconductor alloys such as CVD-grown SiGe,¹¹ MBE-grown InGaAs^{12,13} and, more recently, for the InGaP/GaAs system grown by the chemical beam epitaxy (CBE).^{14–16} Moreover, both theoretical^{17–22} and experimental^{11,12,18,20} works have shown that lattice mismatch of film/substrate and even compositional variations

within the layer play an important role in the morphology of growing semiconductor alloy films. The conditions of coupling between morphological and compositional instabilities have been rigorously established theoretically.^{19,22}

From the application point of view, the existence of such bulk phenomena coupled to surface morphological instabilities can change both optical and electrical behaviors of the alloy films and, consequently, the successful performance of devices based on them. In spite of that, we have recently shown that periodic compositional modulation can be applied to control the lateral positioning of self-assembled nanostructures.^{15,16} Thus the understanding of bulk phenomena, as well as surface morphology, becomes a crucial goal for heterostructure design using semiconductor alloys.

Compositional modulation in such alloys has been previously associated to the phenomenon of spinodal decomposition, in which a minimization of the solid solution free energy leads to phase separation in the material. Actually, compositional modulation in LPE-grown InGaAsP films^{9,10} occurred precisely in the temperature range predicted by the spinodal decomposition diagram calculated by Cremoux *et al.*²³ However, these predicted critical temperatures for the spinodal decomposition are found to be much lower than the typical substrate temperatures for growth techniques working away from thermodynamic equilibrium such as MBE.¹³ Additionally, bulk diffusion is expected to be negligible.²⁴ In particular, Glas¹⁷ proposed a thermodynamical approach to address joint morphological and compositional instabilities. In this model, unstable joint modulation and undulations exist at any temperature. This analysis, however, does not consider kinetic limitations for the system of interest. More recently, alternative theoretical models^{13,18–22} have considered surface mechanisms as well as stress-driven effects to explain the growth dynamics of binary or pseudo-binary semiconductor alloys, such as SiGe and InGaAs, respectively. In

^{a)}Present address: Campus Experimental de Sorocaba, GPM, UNESP, 18087-180 Sorocaba-SP, Brazil. Electronic mail: jrborto@sorocaba.unesp.br

^{b)}Present address: Department of Physics, Penn State University, University Park, PA 16802.

this context, these alloys are generically named *AB* alloys, where *A* and *B* stand for the two species constituting the alloy.

The model proposed by Leonard and Desai²⁰ predicts the dynamics of the free surface and the composition nonuniformities in strained *AB* alloys taking into account surface spinodal decomposition and kinetic mechanisms. Surface diffusion is the dominant mass transport mechanism, and the total flux of material diffusing on the surface is proportional to the gradient of a composition-weighted chemical potential. The difference in the size of *A* and *B* atoms induces stresses in the bulk, which in turn drive the surface mechanisms. The coupling of misfit strain, compositional stress, deposition rate, and growth temperature determine the stability of film morphology as well as the compositional modulation.

On the other hand, the model proposed by Spencer *et al.*^{21,22} predicts the dynamics of composition and morphology in *AB* alloy films by considering the coupling of misfit and solute strains as well as the kinetic influence of species-dependent surface mobilities. First, this model considers the stresses due to misfit and to composition gradients when *A* and *B* present different atomic sizes. Consequently, stress and composition become coupled. For mass transport, similarly to the model by Leonard and Desai, the dominant mechanism is surface diffusion, with crystal growth occurring by a generic uniform growth rate. However, *A* and *B* species can diffuse independently on the growing surface. This allows surface diffusion to be species dependent, although isotropic. More precisely, surface diffusion of each component is achieved separately in response to the chemical potential gradient. Finally, the chemical potentials for each species are derived in terms of surface energy, strain, and composition.

These models share the assumption that surface microscopic mechanisms can lead to a larger scale phenomena such as compositional modulation. Both models consider a generic substitutional *AB* alloy with an atomically rough surface and describe the evolution of surface and composition nonuniformities using conservation of atomic species. The model by Leonard and Desai predicts stability for both compressive and tensile strain, with composition and morphology always coupled. Thus, a planar surface can be achieved only if alloy decomposition is suppressed and vice versa. On the other hand, the model by Spencer *et al.* predicts that stable growth takes place for compressive misfits when one component is large and slow relative to the other; and for tensile misfits when one component is large and fast relative to the other. This remarkable discrepancy between these models has been credited to the kinetic influence of species-dependent surface mobilities.^{21,22} Thus, from the experimental point of view, one can expect that the surface diffusivities of *A* and *B* species should play important roles both on surface morphology and bulk properties of semiconductor alloys.

The kinetic mechanisms are indeed present on the surface during growth by MBE-like techniques. The direct measurement of mean free path for the surface diffusion of the different atomic species still presents a challenge from the experimental point of view. However, the validation of these

mechanisms is usually done by direct comparison of surface parameters such as roughness, fractal dimension, scaling coefficients, and morphological features (measured experimentally) with those predicted by theoretical models, since many important characteristics of the alloys as well as the influence of the growth conditions on those characteristics can be derived from these models. These predictions, however, are not the same for different models; our goal with this work is to provide experimental data allowing the further development of these models.

In this work, we address the role of surface diffusion on the formation of different compositional profiles and surface morphologies in InGaP alloys grown on (001) GaAs substrates by CBE. In this context, the influence of surface step density and In content were both investigated. InGaP films with compressive strain and grown under different conditions were studied. Special emphasis was made on the influence of the V/III ratio (in the gas supply) during InGaP layer deposition, since it strongly affects surface reconstruction. The structural characterization, carried out by transmission electron microscopy (TEM) and atomic force microscopy (AFM) measurements, shows that compositional modulation can give rise to surface instabilities while CuPt-type atomic ordering is correlated with the formation of bilayer-high terraces on the growing surface. Moreover, we also observed that compositional modulation is not always coupled to surface instabilities, and smooth InGaP films with periodic compositional variation along the surface could thus be obtained. The influence of surface reconstructions as well as surface step density and In content on the final growth characteristics can be accommodated by theoretical models in literature^{21,22} if modification of In and Ga relative surface mobilities occurs.

II. EXPERIMENTAL SETUP

The samples were grown by chemical beam epitaxy (CBE) on both nominally oriented and misoriented (2° toward $\langle 111 \rangle_A$, *A*-surface hereafter) semi-insulating (001) GaAs substrates. Trimethylindium and triethylgallium, with H₂ as a carrier gas, were used as group-III sources. Thermally cracked AsH₃ and PH₃ were used as group-V sources. The substrate native oxide was removed by heating the sample at 600 °C under AsH₃ overpressure. For all samples presented here, a 300 nm GaAs buffer layer at 550 °C and growth rate of 0.72 μm/h, followed by a 400 nm InGaP layer at a rate of 0.95 μm/h were grown. During InGaP growth, the V/III ratio was varied from sample to sample in the range of 10–32, by only changing the PH₃ flux. The lattice mismatch between the In-rich InGaP and GaAs films, ranging from 0% to 0.9%, was controlled by varying the In/Ga ratio through the modification of TMI flux. Run-to-run fluctuations in the InGaP composition provided mismatch variations smaller than 0.05%. The mismatch values were measured from (004) rocking curves using double-crystal x-ray diffractometry (XRD). Surface morphology was characterized using AFM in-air, operating in a noncontact mode. Silicon conical tips with 5 nm typical radius of curvature supported by cantilevers with resonance frequencies around

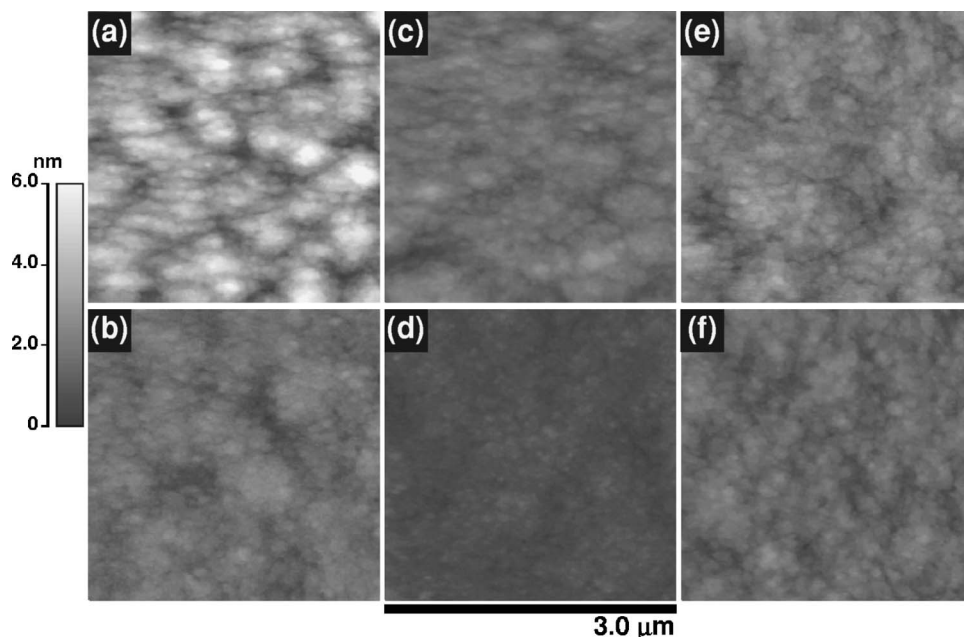


FIG. 1. $3\ \mu\text{m} \times 3\ \mu\text{m}$ AFM images of lattice matched (upper row) and In-rich (lower row) InGaP/GaAs films. The lattice mismatch in In-rich InGaP layers is in the range from 0.45% to 0.65%. The growth temperature and V/III ratio during InGaP deposition for each run were: (a) and (b) $540\ ^\circ\text{C}$ and 17, (c) and (d) $550\ ^\circ\text{C}$ and 17, and (e) and (f) $550\ ^\circ\text{C}$ and 32. All images are shown in the same height scale. From (a) to (f), the rms roughness for the AFM images are 1.09, 0.40, 0.39, 0.20, 0.53, and 0.38 nm, respectively.

80 kHz and spring constant ranging from 1.8 to $3.2\ \text{N/m}$ were used. All AFM scans were taken with 256×256 data points. The film surface roughness was derived from AFM scans by calculating the root mean square (rms) roughness

w_{rms}

$$w_{\text{rms}} = \sqrt{\frac{1}{N} \sum_{i=1}^N (h_i - \bar{h})^2},$$

where N^2 is the number of pixels, h_i is the height in each point, and \bar{h} is the surface mean height along the AFM scan. Transmission electron diffraction (TED) patterns and dark-field TEM images were acquired using a JEM 3010 URP 300 kV TEM. The XRD and TEM measurements indicate that all samples discussed here are dislocation free. Reflection high-energy electron diffraction (RHEED) was carried out *in situ* on the growing surfaces, using an electron gun operated at 20 keV.

III. RESULTS AND DISCUSSION

Figure 1 summarizes the influence of growth conditions (Indium content, temperature, and the V/III ratio) on the InGaP surface morphology measured by AFM. Figures 1(a), 1(c), and 1(e) correspond to films lattice-matched to GaAs while Figs. 1(b), 1(d), and 1(f) are mismatched InGaP/GaAs films ($\varepsilon=0.45\text{--}0.65\%$). The growth temperature and V/III ratio during InGaP deposition for each run were: Figures 1(a) and 1(b)— $540\ ^\circ\text{C}$ and 17, Figs. 1(c) and 1(d)— $550\ ^\circ\text{C}$ and 17, and Figs. 1(e) and 1(f)— $550\ ^\circ\text{C}$ and 32. The AFM images exhibit rms roughness in the range of 0.2–1.1 nm, depending on growth conditions. We can clearly notice from the height variation in Fig. 1 that the mismatched InGaP films are smoother, in spite of the higher strain. Another interesting feature in the AFM images [Figs. 1(a) and 1(b)] is the presence of mounds, or isotropically shaped three dimensional (3D) surface structures. The mounds present larger lateral size and smaller heights when the In content is increased (strained layers). Mound formation in homoepitaxial

films has been attributed to the presence of kinetic barriers, particularly at step edges;^{25,26} in our case, the results shown in Fig. 1 indicate that diffusion bias mechanisms play an important role on the surface roughness. Thus, higher temperatures should promote smoother InGaP surfaces, as indeed is observed in Figs. 1(c)–1(f), since all surface kinetic mechanisms are thermally activated.^{25,26} Actually, in our case a small increase in temperature ($10\ ^\circ\text{C}$) is enough to prevent mound formation. Moreover, comparing Figs. 1(a) and 1(c) with Figs. 1(b) and 1(d), respectively, we can notice that strained film surfaces are even smoother than those of lattice-matched material. This is one of the subjects of investigation in our work.

The presence of morphological, as well as compositional instabilities in semiconductor alloys, has been reported by several works in literature as strongly dependent on growth parameters such as temperature and lattice mismatch.^{12,13,18} We have recently reported¹⁶ that compositional modulation in InGaP films grown by CBE depends on the growth temperature and In content. Furthermore, our previous results have also pointed out that the V/III ratio plays an important role on this bulk phenomenon. In order to better understand these results, we have performed TEM and AFM measurements in a set of InGaP films where the V/III ratio was varied from 32 to 10, while growth temperature and mismatch were kept at $550\ ^\circ\text{C}$ and (0.68–0.05)%, respectively.

Cross-sectional $g=(2-20)$ dark-field TEM images of InGaP films grown with a decreasing V/III ratio are shown in Fig. 2. We can observe that the compositional modulation becomes stronger when the V/III ratio is reduced. Moreover, Figs. 2(b) and 2(c) show that the dark/bright contrast period, and consequently the characteristic length of compositional modulation, becomes shorter.

With respect to the surface morphology, Fig. 3 shows the AFM images for this same set of InGaP films, grown with the decreasing V/III ratios. The rms roughness associated to each surface as a function of the V/III ratio used for InGaP growth is displayed in Fig. 4. When the V/III ratio is greater

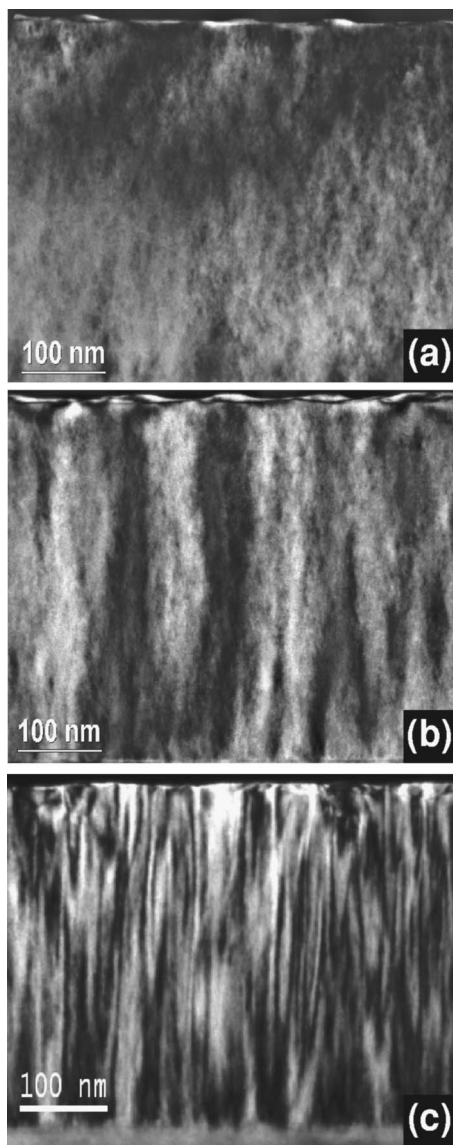


FIG. 2. Cross-sectional $g=(2-20)$ dark-field TEM images of the InGaP layers grown at a temperature of 550 °C and V/III ratio of (a) 32; (b) 17, and (c) 10. The periodic dark/bright contrast on samples B and C is associated with compositional modulation.

than 17, surface morphology is dominated by the presence of large terraces, mainly bilayer-high [Fig. 3(f)]. On the other hand, when V/III is equal to 10, a surface corrugation up to 10 nm high can be observed on the top of the InGaP film. The spatial orientation of this two-dimensional periodic corrugation is essentially the same shown by the periodic strain field related to the compositional modulation.¹⁶ Both are roughly aligned at [010] and [100] crystallographic directions as shown in the inset of Fig. 3(e) by the anisotropic intensity distribution in the fast Fourier transform image. This similarity suggests that a morphological instability is coupled to the compositional modulation when the latter is stronger, as predicted theoretically.¹⁹⁻²²

In the transition region between these two behaviors, the surface of the sample grown at the V/III ratio equal to 17 presents neither large bilayer-high terraces nor periodic corrugation. In fact, monolayer-high terraces with small areas are observed in the morphology. As a consequence, its sur-

face roughness corresponds to the minimum value in Fig. 4, approximately 0.20 nm. This value is even smaller than the typical roughness measured for GaAs buffer films, about 0.30 nm. Thus AFM and TEM results taken together clearly show that compositional modulation is not necessarily coupled to surface instabilities, even for relatively thick films (in our case, approximately 400 nm). Previous experimental data reported in literature¹¹⁻¹³ always associate compositional modulation with large surface roughness, contrarily to our results. At certain growth conditions (550 °C, V/III ratio=17 and strained mismatch in the range of 0.6–0.8% for our experiment), it is possible to obtain compositional modulated InGaP films with smooth surfaces in a reproducible way. Actually, the InGaP surface roughness can be lower than that observed for GaAs even when the strain field related to compositional variations and lattice mismatch is large enough to spatially order InP islands grown on top of the InGaP film.¹⁵

Figure 4 also shows an important result: Maximum and minimum roughness values are observed for different surface reconstructions, according to reflection high-energy electron diffraction (RHEED) measurements. The formation of the bilayer-high terraces, observed in the topography of samples exhibiting (2×1) surface reconstruction, has been related to $[1-10]$ P dimerization due to P_2 excess on the growing InGaP surface.^{6,7} Moreover, their presence has also been correlated with CuPt_B ordering in InGaP films.^{6,7,14} This is also the case for our samples, as shown by TED patterns and $[110]$ cross-sectional dark-field TEM images taken with $g=(1/2, 1/2, 1/2)$ excitation. Figure 5 shows these TEM measurements for different growth conditions of In-rich InGaP layers; Fig. 5(a) shows ordered domains up to 20 nm in size. However, atomic ordering is almost absent on the InGaP sample where compositional modulation is stronger [Fig. 5(b)]. The degree of ordering scales with P_2 overpressure, since ordered domains can be observed for lower growth temperatures [Fig. 5(a)] or larger V/III ratios [Fig. 5(c)]. The size and position of these domains are randomly distributed along the layer. The same behavior is observed for InGaP films lattice-matched to GaAs substrates; the volume of ordered regions appears to be independent of the mismatch between the InGaP film and the GaAs substrate.

However, when the surface reconstruction is purely (2×4) , neither CuPt_B domains nor bilayer-high terraces are observed. At the same time, the InGaP layer exhibits strong compositional modulation and periodic corrugations on the surface, in agreement with theoretical predictions¹⁹⁻²² and previous experimental reports.¹¹⁻¹³ Additionally, our results show that there is a transition region in the RHEED pattern, where pure (2×1) or (2×4) reconstructions are not observed—instead a diffuse pattern shows up on screen. Samples grown at these conditions show the presence of compositional modulation and smooth surfaces, with no bilayer-high terraces. These are the technologically relevant samples since their periodic strain field may be used as a template for the design of new structures, as we have shown for the case of quantum dot positioning.^{15,16}

The characteristic length of surface and subsurface mechanisms leading to atomic ordering and compositional

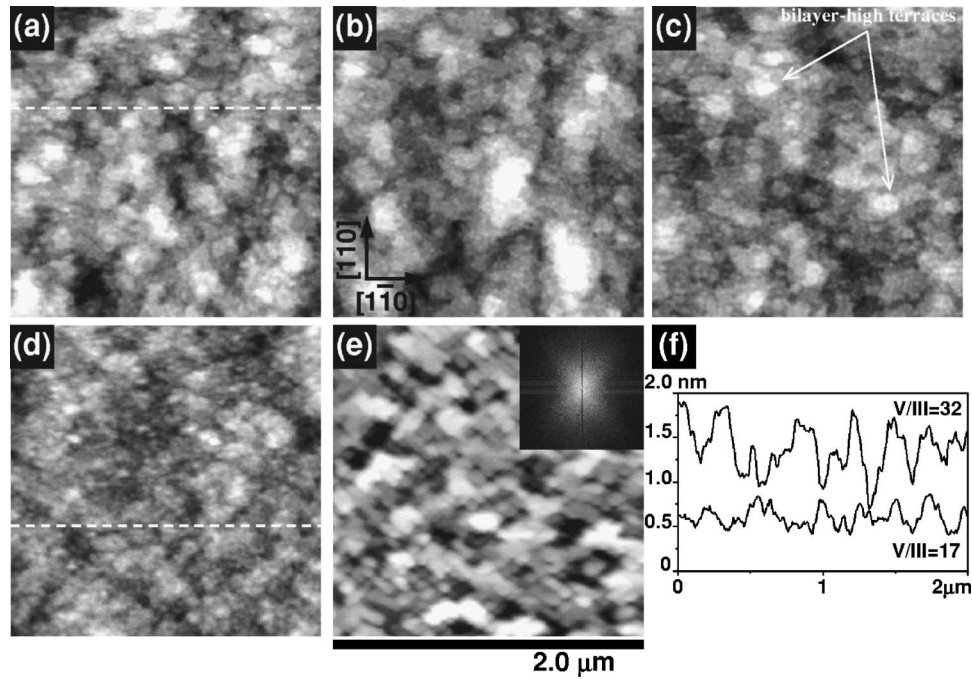


FIG. 3. $2\ \mu\text{m} \times 2\ \mu\text{m}$ AFM images of In-rich InGaP layers grown with different V/III ratios: (a) 32, (b) 27, (c) 22, (d) 17, and (e) 10. From (a) to (e), the height variation range and rms roughness (in parentheses) for the AFM images are 2.95 (0.39), 3.17 (0.46), 2.11 (0.29), 1.39 (0.17), and 23.27 nm (3.18 nm), respectively. The inset in part (e) presents the two-dimensional FFT image for a $4 \times 4\ \mu\text{m}^2$ for the same sample, showing the anisotropic intensity distribution associated to the periodic corrugation. The growth temperature was maintained at $550\ ^\circ\text{C}$ during InGaP deposition and strained mismatch is $(0.68 \pm 0.05)\%$ for all samples. Part (f) shows typical profiles from AFM images of InGaP grown at the V/III ratio equal to 32 and 17. These profiles are indicated by dashed lines on parts (a) and (d), respectively. Two typical bilayer-high terraces (with a step height of approximately two monolayers, or 0.6 nm) present on the InGaP surface when the V/III ratio is >17 were used are indicated on part (c).

modulation are quite different. The former can be associated to lengths in the scale of the lattice parameter, while the latter is at least two orders of magnitude larger. Surface reconstruction could be expected to affect adatom diffusivities, since adsorbed species can show surface diffusion lengths in the nm range.^{27,28} It is not unexpected that this parameter presents a strong effect on compositional modulation, according to the models describing these phenomena.^{18–22}

Since direct measurements of adatom surface diffusion lengths are quite challenging, we might get some insight into this problem by looking at the effect of different parameters on our samples. For example, surface step density is known

to directly affect the overall surface diffusion, by providing stable sites for adatom incorporation or extra energy barriers to adatom movement on the surface.²⁹ We thus investigated the role of vicinal surfaces on morphological instabilities, keeping in mind the TEM results presented in Fig. 2 as well as in literature; Peiró *et al.*^{30,31} have shown that vicinal substrates can enhance the degree of compositional modulation and surface undulations on InAlAs/InP and InGaAs/InP sys-

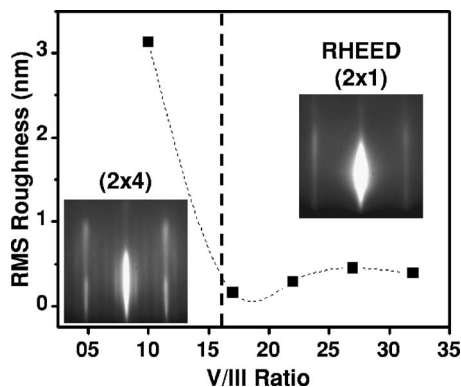


FIG. 4. Relationship between the rms roughness and the V/III ratio during growth of the InGaP layer. The rms roughness was calculated from AFM images displayed on Fig. 3. RHEED patterns taken in the azimuth $[1-10]$ are shown in insets. The vertical dashed line divides the V/III ratio values so that surface reconstruction is mainly 2×4 and 2×1 during InGaP growth.

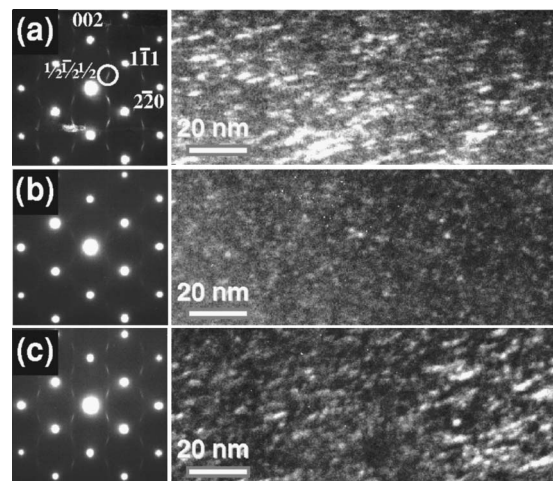


FIG. 5. TED patterns and $[110]$ cross-sectional dark-field TEM images taken with $g=(1/2, 1/2, 1/2)$ excitation of the InGaP layers grown at different conditions. The growth temperature and V/III ratio for each run were: (a) $540\ ^\circ\text{C}$ and 17, (b) $550\ ^\circ\text{C}$ and 17, and (c) $550\ ^\circ\text{C}$ and 32. The AFM images of these InGaP layers are shown on Figs. 1(b), 1(d), and 1(f), respectively.

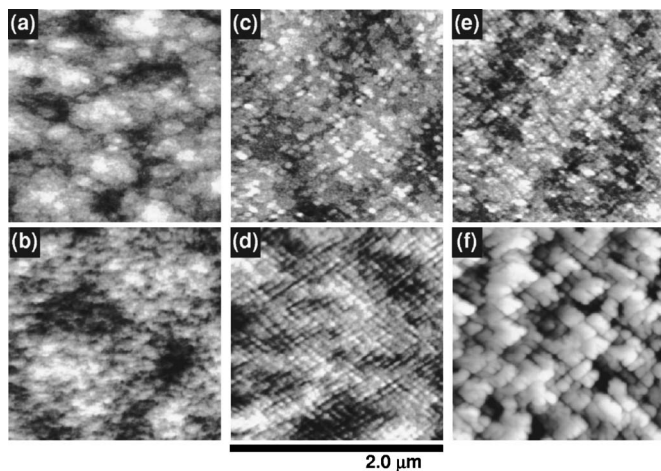


FIG. 6. $2\ \mu\text{m} \times 2\ \mu\text{m}$ AFM images of InGaP/GaAs films grown simultaneously on nominal (upper row) (e) A-surface (lower row) substrates. The strained mismatch on InGaP/GaAs films is about (a) and (b) 0%, (c) and (d) 0.67%, and (e) and (f) 0.89%. All InGaP layers were grown at $550\ ^\circ\text{C}$, $V/\text{III}=17$, and with a thickness about 400 nm. The rms roughness of AFM images are 0.37, 0.61, 0.25, 0.69, 0.25, and 2.83 nm, respectively. From (a) to (f), the height variation range and rms roughness (in parentheses) for the AFM images are 2.77 (0.37), 4.30 (0.61), 1.99 (0.25), 5.04 (0.69), and 21.17 nm (2.83 nm), respectively.

tems grown by MBE. In our case, Fig. 6 shows that the periodic corrugation formation is also enhanced when vicinal A-surface substrates are used. For example, the AFM image shown in Fig. 6(c) displays only a few structures (with steps up to 0.6 nm) distributed along a faint two-dimensional array. Figure 6(d), however, shows a more striking surface structure, where a surface corrugation up to 1 nm high can be observed. This corrugation exhibits a two-dimensional periodicity; its period (70 nm) is essentially the same as that for compositional modulation.¹⁶ Figure 6(f) shows that growth has reached the instability regime, with a huge increase in surface roughness compared to samples grown under smaller strain on vicinal surfaces.

This trend of increasing roughness and array formation also occurs when a larger In flux is used for growth, thus increasing the strain in the layer. However, even larger strain values for samples grown at $540\ ^\circ\text{C}$ do not trigger the change in morphology.³² The dependence on temperature is then more relevant to the roughening process, suggesting that diffusion is indeed the main mechanism for the morphology formation. We should point out, however, that a larger In flux during growth at a fixed temperature must necessarily change the relative In/Ga population of adatoms on the surface. Thus a larger In population on the surface can be expected during growth of the more mismatched materials.

Our experimental results thus show a correlation between surface reconstruction and morphologies, which are also affected by growth parameters such as vicinal substrates or larger In flux. The trend in morphology is similar for samples shown in Figs. 3 and 6. Once bilayer-high terraces are no longer observed, smooth morphologies take place in the transition from (2×1) to (2×4) in the RHEED pattern. This transition alone may implicate in changing surface dynamics, by affecting surface diffusion as shown, for example, by RHEED measurements on GaAs surfaces.³³ Moreover, at

this transition region, increasing the In flux or using A-surfaces for growth provide morphologies with periodically arranged terraces and, at extreme conditions, periodically corrugated surfaces with larger height variation. Both structures are aligned at $[100]$ and $[010]$ directions, as seen in Figs. 3(e) and 6(f).

The presence of larger step densities on the growing surface should affect adatom surface diffusion but not surface reconstruction. Figures 6(b), 6(d), and 6(f) clearly show that the trend in morphology described above develops more easily on stepped surfaces. We cannot obtain from our experimental results a microscopic view of each group III—adatom diffusivity or how it is actually affected by the chosen growth parameters. However, if we take into account the theoretical models dealing with compositional modulation, our data could be more suitably described by that from Spencer *et al.*^{21,22} This model allows the possibility of uncoupled instabilities in morphology and compositional modulation for compressively strained films, as we observe at the transition region. However, it also imposes constraints on group III diffusivities according to the atom size. According to this model, and the fact that the InP lattice parameter is larger than GaP, compressive InGaP surfaces could be smooth and stable if the surface mobility of Ga adatoms is larger than In adatoms. From the energetics point of view, this hypothesis may be unexpected since Ga surface bonds should be more stable than In for binary alloys. However, our experimental system is much more complex; our data shows that InGaP is not a pseudo-binary alloy as considered by most theoretical models. This rather complex scenario where one species surface concentration may affect or hinder another species incorporation has been shown by several authors in the past.^{34,35} Our experimental results point to an effect of surface relaxation processes—diffusion in particular—to the behavior reported here for our InGaP samples. Indeed, Fig. 6 shows that instability is reached faster for larger In/Ga relative adatom populations and larger step densities. Thus a relative change in In/Ga surface diffusivities may occur, in the sense of decreasing eventual differences originated from energetic considerations. Whatever the actual microscopic mechanisms are, their experimental observation is rather difficult and can hardly be quantitatively predicted.

IV. CONCLUSIONS

In summary, our results indicate that surface diffusion is the main driving mechanism for compositional modulation on InGaP films grown by CBE. In this sense, surface reconstruction shows a strong effect on both compositional modulation and the CuPt_b atomic ordering phenomena. When the RHEED pattern displays the (2×1) surface reconstruction, the bulk of the InGaP layer presents only CuPt_b domains. In this situation, compositional variations are not observed. Contrarily, when the RHEED pattern displays the (2×4) surface reconstruction, the InGaP layers exhibit compositional modulation instead of atomic ordering. In the transition from (2×4) to (2×1) reconstruction, InGaP films exhibit both compositional modulation and atomic ordering phenomena, although the latter is very weak.

Moreover, the surface morphology is intrinsically related to these bulk phenomena. In the regime where CuPt_B ordering is stronger, the surface presents bilayer-high terraces morphological structures. Otherwise, surface morphology is basically formed by a two-dimensional surface corrugation. This corrugation is coupled to periodic composition variations inside the layer via the strain field. In the transition between these two regimes, however, the surface presents neither one of the former types of structures and, consequently, is very smooth. This result indicates that compositional and morphological instabilities are not necessarily coupled. From the application point of view, these InGaP films can be used as a template to the deposition of strained films, changing the deposition dynamics and henceforth creating spatially ordered nanostructure systems.

From theoretical models available on literature, a likely explanation for the surface reconstruction effect on InGaP compositional modulation is through changes in In/Ga adatom relative diffusivities. More strictly, P_2 overpressure could alter the relative diffusion of In and Ga adatoms during InGaP growth. This assumption is in agreement with the uncoupled compositional and morphological instabilities observed in our experimental set.

ACKNOWLEDGMENTS

This work was supported by the Brazilian Agencies FAPESP, CNPq, and FINEP. Two of the authors (J.R.R.B. and H.R.G.) acknowledge financial support from FAPESP. TEM measurements were carried out at the LME facilities of the Brazilian Synchrotron Light Laboratory (LNLS), Brazil. We also thank R. Marcon for technical assistance with the XRD measurements and J. G. Zelcovit for TEM sample preparation.

¹T. Takamoto, E. Ikeda, H. Kurita, and M. Ohmori, *Appl. Phys. Lett.* **70**, 381 (1997).

²K. Häusler, K. Eberl, F. Noll, and A. Trampert, *Phys. Rev. B* **54**, 4913 (1996).

³W. Seifert, N. Carlsson, A. Petersson, L.-E. Wernersson, and L. Samuelson, *Appl. Phys. Lett.* **68**, 1684 (1996).

⁴H. Lee, J. A. Johnson, M. Y. He, J. S. Speck, and P. M. Petroff, *Appl. Phys. Lett.* **78**, 105 (2001).

⁵O. Ueda, M. Takikawa, J. Komeno, and I. Umebu, *Jpn. J. Appl. Phys.* **26**, L1824 (1987).

⁶S. H. Lee and G. B. Stringfellow, *J. Appl. Phys.* **83**, 3620 (1998).

⁷Y. S. Chun, S. H. Lee, I. H. Ho, and G. B. Stringfellow *J. Appl. Phys.* **81**,

646 (1997); Y. S. Chun, H. Murata, T. C. Hsu, I. H. Ho, L. C. Su, Y. Hosokawa, and G. B. Stringfellow, *ibid.* **79**, 6900 (1996).

⁸N. Liu, C. K. Shih, J. Geisz, A. Mascarenhas, and J. M. Olson, *Appl. Phys. Lett.* **73**, 1979 (1998).

⁹P. Henoc, A. Izrael, M. Quillec, and H. Launois, *Appl. Phys. Lett.* **40**, 963 (1982).

¹⁰O. Ueda, S. Isozumi, and S. Komiya, *Jpn. J. Appl. Phys., Part 2* **23**, L241 (1984).

¹¹T. Walther, C. J. Humphreys, and A. G. Cullis, *Appl. Phys. Lett.* **71**, 809 (1997).

¹²T. Okada, G. C. Weatherly, and D. W. McComb, *J. Appl. Phys.* **81**, 2185 (1997).

¹³D. González, G. Aragon, D. Araújo, and R. Garcia *Appl. Phys. Lett.* **76**, 3236 (2000); D. González, G. Aragon, D. Araújo, M. J. de Castro, and R. Garcia, *ibid.* **74**, 2649 (1999).

¹⁴J. Bettini, M. M. G. de Carvalho, M. A. Cotta, and D. Ugarte, *Surf. Sci.* **540**, 129 (2003).

¹⁵J. R. R. Bortoleto, H. R. Gutiérrez, M. A. Cotta, J. Bettini, L. P. Cardoso, and M. M. G. de Carvalho, *Appl. Phys. Lett.* **82**, 3523 (2003).

¹⁶J. R. R. Bortoleto, H. R. Gutiérrez, M. A. Cotta, and J. Bettini, *Appl. Phys. Lett.* **87**, 013105 (2005).

¹⁷F. Glas, *Phys. Rev. B* **55**, 11277 (1997).

¹⁸J. E. Guyer, S. A. Barnett, and P. W. Voorhees, *J. Cryst. Growth* **217**, 1 (2000).

¹⁹F. Léonard and R. C. Desai, *Appl. Phys. Lett.* **74**, 40 (1999).

²⁰Z.-F. Huang and R. C. Desai, *Phys. Rev. B* **65**, 205419 (2002).

²¹B. J. Spencer, P. W. Voorhees, and J. Tersoff, *Appl. Phys. Lett.* **76**, 3022 (2000).

²²B. J. Spencer, P. W. Voorhees, and J. Tersoff, *Phys. Rev. B* **64**, 235318 (2001).

²³B. de Cremoux, P. Hirtz, and J. Ricciardi, in *GaAs and Related Compounds, Vienna 1980*, edited by H. W. Thim (Institute of Physics, London, 1981).

²⁴T. McDevitt, S. Mahajan, D. E. Laughlin, W. A. Bonner, and V. G. Keramidis, *Phys. Rev. Lett.* **45**, 6614 (1992).

²⁵P. Smilauer and D. D. Vvedensky, *Phys. Rev. B* **49**, 5769 (1994).

²⁶J. R. R. Bortoleto, M. A. Cotta, and M. M. G. de Carvalho, *Surf. Sci.* **515**, 117 (2002).

²⁷D. J. Arent, S. Nilsson, Y. D. Galeuchet, H. P. Meier, and W. Walter, *Appl. Phys. Lett.* **55**, 2611 (1989).

²⁸M. P. P. de Castro, N. C. Frateschi, J. Bettini, and M. M. G. de Carvalho, *J. Cryst. Growth* **193**, 510 (1998).

²⁹T. Shitara, D. D. Vvedensky, M. R. Wilby, J. Zhang, J. H. Neave, and B. A. Joyce, *Phys. Rev. B* **46**, 6815 (1992).

³⁰F. Peiró, J. C. Ferrer, A. Cornet, M. Calamitoutou, and A. Georgakilas, *Phys. Status Solidi A* **195**, 32 (2003).

³¹F. Peiró, A. Cornet, J. R. Morante, A. Georgakilas, C. Wood, and A. Christou, *Appl. Phys. Lett.* **66**, 2391 (1995).

³²J. R. R. Bortoleto, H. R. Gutiérrez, J. Bettini, and M. A. Cotta (unpublished).

³³J. M. van Hove and P. I. Cohen, *J. Cryst. Growth* **81**, 13 (1987).

³⁴N. Kobayashi, J. L. Benchimol, F. Alexandre, and Y. Gao, *Appl. Phys. Lett.* **51**, 1907 (1987).

³⁵J. F. Carlin, A. Rudra, and M. Ilegems, *J. Cryst. Growth* **131**, 387 (1993).